MATRIX-FRACTURE INTERACTIONS DURING GAS INJECTION: A PORE-SCALE EXPERIMENTAL STUDY

M. Sabti, A.H. Alizadeh, and M. Piri
Department of Petroleum Engineering, University of Wyoming,
1000 E. University Ave., Laramie, WY 82071-2000, USA

This paper was prepared for presentation at the International Symposium of the Society of Core Analysts held in Snow Mass, Colorado, USA, 21-26 August 2016

ABSTRACT

Fractured oil reservoirs represent a massive percentage of hydrocarbon formations in the world. Improvement in oil recovery from these reservoirs can be achieved by developing a better understanding of interactions between matrix and fracture and governing mechanisms at the pore level. X-ray micro-computed tomography (CT) imaging techniques can be employed to explore the underlying physics by mapping fluid pore occupancies in matrix and fracture during displacements. The main scope of the present study is to examine the possible beneficial role of spreading phenomena in transferring oil from matrix to fracture during gas injection.

We systematically investigate pore-scale displacement physics of three-phase (*i.e.*, brine, oil, and gas) flow in fractured porous media and the effectiveness of interaction mechanisms between matrix and fracture using spreading oil. The study is performed based on comparing pore fluid occupancies at a wide range of oil saturations in the pore space established by injecting gas. Visualizing the pore configurations at different oil saturations in the medium reveals the substantial role of spreading layers in maintaining the hydraulic conductivity and the phase connectivity of oil from the matrix to the fracture during the displacement. This mainly takes place at higher gas flow rates where layer drainage in the presence of stable spreading oil layers is the dominant displacement mechanism. At lower gas flow rates, however, the oil displacement is primarily governed by the accessibility of the gas to pore elements adjacent to the fracture as well as threshold capillary pressure.

INTRODUCTION

Fractured reservoirs host a significant percentage of oil reserves in the world, particularly in the Middle East [1]. They are one of the most complicated groups of heterogeneous geological structures that can be either natural due to earth stresses or artificial due to the drilling operations or hydraulic fracturing. Hydrocarbon recovery from these reservoirs is amongst the most challenging processes in the oil industry. The complexity of such systems is amplified when the fractures are highly conductive and behave as conduits carrying most of the fluid that in turn prevents the build-up in pressure gradient across the reservoir matrix. To deal with such conditions, one needs to develop a better understanding of the governing pore-scale physics and improve the efficiency of the

injection schemes. As an example, it is believed that during gas injection into fractured reservoirs, gas would easily flow through the fractures and hence might not effectively invade the matrix, causing poor sweep efficiency of oil [2]. However, there might be circumstances under which the efficiency of such scenarios can be improved.

Similar to non-fractured media, flow of fluids and consequent recovery trends in fractured porous media are strongly affected by matrix-fracture interactions and rock-fluid and fluid-fluid characteristics, such as wettability and interfacial tension, as well as multi-phase flow properties, such as capillary pressure and relative permeability [3, 4]. Several experimental studies presented in the literature [3-5] were aimed at understanding matrix-fracture interactions and the mechanisms of flow to improve recovery factors. Despite the substantial contributions of these studies, the physics of displacement mechanisms responsible for matrix-fracture interactions are still uncertain and poorly understood. This might be due to the complexities of fracture morphology and/or the limitations of experimental technology. As an example, one of the drawbacks of studying fractures using medical CT scanners is the limitation in resolution. The fracture aperture would often be too small to be visualized with the employed resolution, and hence, fluid occupancies in the fractures could not be mapped accurately. The advent of high-resolution micro-CT scanners, however, has helped mitigate these deficits as it provides researchers with much superior imaging resolutions to map the fluid occupancies at the pore scale [6].

Arshadi *et al.* [3] studied matrix-fracture interaction physics under two-phase flow conditions in fractured Berea sandstone using an X-ray micro-CT scanner. The authors investigated the effect of flow rate, aperture geometry, and oil-brine interfacial tension (IFT) on multiphase flow through matrix pores and fracture opening and their interactions. They concluded that IFT and the aperture geometry had significant impacts on the displacements. Furthermore, they showed that the brine flowed through three primary paths during imbibition: through wetting layers formed on the walls of the fracture, through the center of the fracture at high flow rates, and through the matrix pores by invading the matrix either from the fracture or from the core inlet depending on the pressure gradient across the sample. Alajmi and Grader [4] studied matrix-fracture interactions under two-phase flow conditions using an X-ray CT scanner in a layered Berea sandstone sample. They artificially induced the fractures at the inlet and at the outlet of two individual core samples in two sets of experiments to observe the diverging and converging flow in the fractures. The authors concluded that the presence of the fracture reduced the breakthrough time and the recovery. Alvarado *et al.* [5] used a third-generation X-ray CT scanner with a resolution of 25 micrometers to characterize the fracture geometry and map phase distributions in Berea sandstone under two- and three-phase (*i.e.*, water, benzyl alcohol, and decane) flow conditions. They digitally separated the fracture to study the fluid distributions only within the fracture. They studied the mobility and the connectivity of the wetting, intermediate-wetting and non-wetting phases by visualizing the fracture space. It was found that decane (representing the non-wetting gas phase) was in the form of large globules occupying most of the fracture

region and surrounded by benzyl alcohol (representing the intermediate-wetting oil phase). They concluded that the ability to map the fluid occupancies in fracture systems during three-phase flow using X-ray CT technique would help understand the matrix-fracture mass transport.

In porous media, fluid displacements under three-phase flow are typically associated with different concepts comparing to single- and two-phase flow conditions [7]. Layer drainage is an important displacement mechanism, which has a significant effect on ultimate fluid occupancy [7-9]. It is a drainage process during which oil is displaced by gas in the presence of water through stable and connected spreading oil layers. In a water-wet system for example, when water, oil, and gas phases coexist, due to interfacial tensions between pairs of fluids and surface wettability of the medium, it is likely for oil to form spreading layers sandwiched between water in the corners and gas in the center of the pore elements [10]. These layers could strongly contribute to the phase continuity and consequently to the recovery of oil [7, 8, 11, 12]. The influence of these layers may also be extended to fractured porous media. However, the contribution of these layers to the flow in fracture systems might be different from that in non-fractured porous medium. It is expected that the layers will help maintain the hydraulic connectivity of oil between fracture and matrix.

In this study, we investigate the effect of spreading phenomena on fluid displacements in a fractured rock under three-phase flow conditions. High resolution micro-CT scanning techniques are used to explore matrix-fracture interactions by mapping the pore occupancies in matrix and fracture during three-phase flow processes.

ROCK AND FLUIDS

A cylindrical Berea sandstone core plug (38 mm in diameter and 100 mm in length) was artificially fractured by applying non-uniform radial stress. The fracture was induced through only half of the core plug length. Subsequently, a miniature core sample, 10 mm in diameter and 40 mm in length, was cut from the fractured core plug using air as a coolant. The miniature specimen was then dried in an oven at 110 ^{o}C for 24 hours to eliminate moisture. The fracture extended over only half of the core sample allowing us to study the pore-scale physics in both fractured and matrix-only sections of the medium. Table 1 lists the dimensions and petrophysical properties of the core sample used in this study. The aqueous solution was prepared using distilled water, 2 wt% $CaCl_2$, 13 wt% NaI, and 0.01 wt% NaN_3. Sodium Iodine and Sodium Azide were added to the brine as a dopant and an anti-bacterial growth agent, respectively. Soltrol 170 was purified using a gravity column filled with alumina and silica gel to eliminate polar components that could cause undesirable wettability alterations [13]. Afterward, 5 vol% 1-iodooctane ($C_8H_{17}I$) was added to the purified Soltrol to prepare the working oil phase. The gas phase was nitrogen with 99.9% purity. Properties of a fluid system [8] similar to the fluid system used in this study are given in Table 2. The concentrations of the dopants added to brine and oil were determined to optimize the contrasts among all phases (*i.e.*, brine, oil, and gas). All fluids were equilibrated in a separator and recirculated through the flow

system (bypassing the core sample) before use. Interfacial tension values of oil-brine, nitrogen-oil, and nitrogen-brine fluid pairs for a similar fluid system [8] are given in Table 3. These values were measured using the pendant drop method at 5.5 MPa resulting in a spreading coefficient very close to zero. This means that the oil phase would spread on brine in the presence of gas (nitrogen).

EXPERIMENTAL APPARATUS

The experimental setup used in this work consisted of three coupled systems, a state-of-the-art, closed-loop three-phase miniature core-flooding system, a high-resolution micro-CT scanner, and a data acquisition system. The core-flooding system included Rosemount® differential pressure transducers with different ranges, a three-phase separator, two accumulators, and six programmable dual-cylinder 5000 Series Quizix® pumps. Three of the pumps were used to inject the fluids into the core sample (*i.e.*, brine, oil, and gas), an overburden pressure pump to maintain a fixed net confining pressure, and the other two pumps to regulate the back pressure and to compensate for the fluctuations in the separator pressure caused by fluid withdrawal/accumulation. All the fluids were injected from the bottom of the core sample (the fractured end of the sample). All wetted parts in the system were made from Hastelloy and other corrosion resistant material. This integrated apparatus was a closed-loop system and hence allowed us to recirculate all fluid for a sufficient period of time (*i.e.*, about 2 days) to achieve thermodynamic equilibrium between the phases and minimize the mass transfer within the pore space. Each fluid was retracted from the separator, at a certain height based on the density of the retracted fluid, and injected into the core sample. The fluids produced from the production lines of the core holder were received by the back pressure pump, which maintained a constant pore pressure during all injection cycles. This pump then sent the fluids to the separator whose pressure was regulated by another pump and its coupled accumulators.

The integrated high-resolution micro-CT scanner system was a VERSA-XRM510™ micro-CT scanner manufactured by Zeiss. It operates by directing a number of projections on the sample as the sample rotates. This is done while both the source and the detector are fixed in their positions determined on the basis of the desired resolution and field of view. The scanning parameters used were identified based on the dimensions of the core sample. A voltage of 100 kV and a power of 9 Watt were used to run the scan. Two magnification objectives (0.4 X and 4X) were utilized. The 0.4 X objective was used to scan the entire sample whereas the 4X objective was used to scan the desired locations with a higher resolution (see Table 4). An ANDOR™ camera was used to manipulate the field of view. The custom-built miniature core holder, made from carbon fiber to minimize the X-ray attenuation, was located inside the micro-CT scanner during all stages of the experiments. The data acquisition system was the third system coupled with the micro-CT scanner and the core-flooding system. It was operated during all stages of the experiments to monitor the differential pressure across the core sample. The pressure data points were recorded every 15 seconds in a log file. A schematic diagram of the experimental setup used in this study is illustrated in Figure 1 [8].

EXPERIMENTAL PROCEDURES

The experiments were carried out at pore pressure and temperature of 3.45 MPa and 20^{o}C, respectively. During each step of the experiments, only one fluid was injected into the core (*i.e.*, an unsteady-state approach). The net confining pressure was 1.4 MPa and was kept constant during all the injection cycles. After mounting the core holder inside the CT scanner, the core was flooded with dry CO_2 to remove air and then vacuumed for 24 hours. Subsequently, a dry scan image from the entire length of the sample was acquired under ambient conditions to be used as a preliminary scan image of the pore space and the fracture aperture. Afterward, the core sample was vacuum saturated with the main (*i.e.*, doped) brine to establish 100% brine saturation. This brine had to be replaced by a low salinity brine (*i.e.*, 2 wt% $CaCl_2$ and 0.01 wt% NaN_3) under the experimental conditions in order to generate an accurate pore space map. This was done because the contrast between the doped brine and the grains in the images was almost identical. After completely displacing the doped brine with the low salinity brine, a wet reference high-resolution scan was obtained while the flow of brine was maintained at a low value. This wet reference scan was obtained under the experimental conditions and used to map the fracture, obtain the porosity distribution, and later measure fluid saturations in the course of the experiments. The core sample was then subjected to an oilflood (with an initial flow rate of 0.01 ml/min) to establish water saturation of 31%. This was achieved by gradually increasing the oil flow rate up to 0.45 ml/min. During drainage, the pressure drop across the core sample was recorded and quick scans were performed approximately every five hours at a low resolution to monitor water and oil saturations. After establishing the desired two-phase initial condition, gas was injected into the core sample at various flow rates to reach different oil saturations. During gas injection (*i.e.*, secondary gas injection, SGI), the fluid saturations were measured in both the fracture and the matrix. One of the most important attributes of the experimental procedure was to keep the fracture aperture fixed in all stages of the experiment. Any variations in the aperture could cause fine grains to migrate through the fracture, which would in turn lead to error in image processing. To prevent this problem, the confining pressure pump was linked to each injection pump in order to maintain the pressure difference between the pore pressure and the confining pressure during all steps of the flow tests.

DATA ANALYSIS

Three locations (*i.e.*, *A*, *B*, and *C*) were selected along the length of the fractured core sample in order to be scanned, as indicated in Figure 2. The distance of each location from the inlet of the core was determined based on the fracture location, which started from the inlet and ended in the middle of the core sample (*i.e.*, 19 mm from the inlet). As shown in Table 5, location *A* represents the fractured section, location *B* represents the area where the fracture ends, and location *C* represents the matrix-only portion of the sample. Identifying such locations allowed us to study the pore-scale physics in three topologically different parts of the sample. Prior to starting the scanning process, an image recipe was prepared for each of the three locations as shown in Table 5. The recipe

consisted of all desired imaging parameters such as the accurate distance between source and detector, source voltage, sample positions, camera binning, resolution, exposure time, type of objective, and the number of projections. These parameters could be retrieved by recalling the saved recipes at any given time during the experiment. After scanning all the locations, XM-Reconstructor software was used to convert the tomography files to raw images ready to be used in any visualization software (*e.g.*, Avizo). The reconstruction process was optimized by adjusting different parameters on the tomography files, such as center shift, beam hardening, and Kernel smoothing filter.

After reconstructing the data, the three-dimensional (3D) image data sets were analyzed using Avizo™ 9.0.1 software. Four major steps of the processing of the data were (1) image filtering and processing, (2) arithmetic processing, (3) segmentation and thresholding, and (4) quantification analysis. The image filtering included the use of non-local means filter on the raw data images to reduce noise and remove artifacts such as salt and pepper while maintaining boundary edges for various phases present in each stage of the flow experiment. After filtering the images, processing carried out by registration of the wet images (flooded images) with the reference scan by matching identical pixel size in order to get an accurate pore map. Arithmetic processing was then performed to combine the flooded image with the extracted registered pore map to obtain the pore space fluid distributions by multiplying the reference image by the flooded image. Afterward, in order to separate the phases, segmentation using a histogram thresholding approach was used to obtain the final label image. Finally, the volume and/or the saturation of each phase were determined. By following these steps, all tomograms from the micro-CT scanner were quantitatively analyzed by the use of image analysis in two and three dimensions. More details about these steps can be found elsewhere [6, 14].

RESULTS AND DISCUSSION

In this section, we present the results of our pore-scale experimental study on the impact of spreading oil layers on fluid displacements, pore fluid occupancies, and matrix-fracture interactions using the micro-CT images obtained during the flow tests. In the following paragraphs, we first discuss the results of drainage by oil injection and pore-scale observations of relevant displacement mechanisms. Subsequently, we show micro-scale images of the pore space during gas injection and highlight the displacement events taking place during the three-phase experiment.

For the primary drainage, oil was injected at an initial flow rate of 0.01 ml/min and then the flow rate was gradually increased to 0.45 ml/min. This resulted in the establishment of an average initial water saturation (S_{wi}) of 31%. At higher oil flow rates, more brine-filled pores were invaded by oil as capillary pressure increased. Because the medium was water-wet, brine formed thin wetting films on the walls of the fracture and resided as layers in the corners of the pores whereas oil occupied the center of the elements as illustrated in Figure 3-A.

After completion of primary oil drainage, gas injection was started at an initial flow rate of 0.015 ml/min and the injected gas initially invaded the fracture due to the negligible gas-oil capillary pressure in the fracture. Once the fracture was filled with gas, the gas pressure was sufficient to overcome the matrix capillary pressure and gas invaded oil-filled pore elements of the matrix. This was because the oil-filled pores were large and had a lower threshold capillary pressure. Higher threshold capillary pressures were needed for gas to invade brine-filled elements as brine primarily resided in smaller pores. Because the oil was spreading in the fluid system used and the gas was the most non-wetting phase, oil formed spreading layers sandwiched between brine in the corners and gas in the center of the pore elements (see Figure 3-B). These spreading layers had a significant role in maintaining the connectivity of oil in the matrix to oil in the fracture. Figure 4 shows gas invasion into a previously oil-filled pore adjacent to the fracture wall during gas injection at a high flow rate. As illustrated on the right side of the figure, the gas displaces most of the bulk oil from the center of the pore, while oil maintains its continuity from the matrix to the fracture through spreading oil layers.

Figure 5 shows the sequence of displacements at various gas flow rates at an arbitrary cross section of the core sample. Figures 5-A and 5-B correspond to low gas flow rates of 0.015 and 0.04 ml/min, respectively, whereas Figures 5-C and 5-D depict the cross section at high gas flow rates of 4 and 7 ml/min, respectively. At low flow rates, gas present in the fracture starts to invade large pore elements in the matrix, which have the lowest gas-to-oil threshold capillary pressure, and displace oil (see the rectangular areas in Figure 5-A). The image on the left side of Figure 5-A shows a pore element that is directly connected to the fracture with oil in the center and immobile brine in crevices. This oil cluster is mobilized into the neighboring element during gas injection as seen on the left side of Figure 5-B. This displacement of oil at low gas flow rates is governed by piston-like displacement. Another observation was that the larger pores connected directly to the fracture were drained earlier than those that were far away from the fracture. This was a consequence of the accessibility of gas to the pores that were directly connected to the fracture. This conclusion was verified by the uneven gas saturation profile in the perpendicular direction to the gas flow direction as illustrated in Figures 5-A and 5-B. Thus, at low gas flow rates, the two main factors affecting the oil displacement in matrix-fracture systems are the threshold capillary pressure and the accessibility of the gas from the fracture to the adjacent pores in the matrix. As the gas flow rate increases (images on the left side of Figures 5-C and 5-D), gas occupies more space in the center of the above-mentioned pore leading to the formation of thinner oil layers that spread over the immobile brine present in the corners of this pore. It is worth mentioning that at higher gas flow rates, the oil saturation in the pore space reduced further due to layer drainage in the presence of stable spreading layers. This shows the prevalence of these layers in three-phase flow at high gas flow rates. However, layer drainage is a relatively slow process. This was observed at the highest gas flow rate (i.e., 7 ml/min) when oil saturation was continuously decreasing during three days of injection until it reached a steady-state condition. Figure 6 shows the saturation path taken during primary oil drainage and gas injection. The points represent fluid saturations measured at

location *C*. It was also found that the oil saturations at location *C* (matrix-only portion) and location *A* (matrix around the fracture) were different at low gas flow rates but became almost the same at high flow rates. This was mainly due to the presence of the fracture that hindered the displacement of oil from the neighboring matrix during the initial stages of the gas-oil capillary pressure build-up. However, as the gas flow rate (*i.e.*, gas-oil capillary pressure) increased, gas had more accessibility to oil residing in farther pore elements of the neighboring matrix, resulting in producing bulk oil from those elements. As a consequence, the oil saturation became uniform across the pore space.

CONCLUSIONS

The significance and the abundance of connected spreading oil layers sandwiched between the invading gas and the immobile brine was studied in a fractured sandstone rock sample. A high-resolution X-ray micro-CT scanner was used to capture detailed maps of the pore space and fluid distributions in the matrix and the fracture under two- and three-phase flow conditions. These maps clearly demonstrated the relevance of spreading phenomena to fluid displacements in the fracture undergoing three-phase flow processes. It was found that, at higher oil saturations, the displacement of oil was governed by the connectivity of the bulk oil in the matrix and also by how close the pore elements were to the fracture wall, whereas at lower oil saturations, the displacement of oil was governed by spreading oil layers that maintained the connectivity of oil in the matrix to oil in the fracture and established the flow of oil from the matrix pores to the fracture. Recovery from fractured reservoirs can be improved by developing better insights into displacement physics at the pore level thereby reducing the uncertainties associated with the design and deployment of appropriate recovery schemes.

ACKNOWLEDGEMENTS

The authors gratefully appreciate the financial support of Saudi Aramco, Hess Corporation, and the School of Energy Resources at the University of Wyoming.

REFERENCES

1. Geiger, S., M. Stephan, “What can we learn from high-resolution numerical simulations of single- and multi-phase fluid flow in fractured outcrop analogues?”, *Advances in the study of fractured reservoirs*, geological society 374. dx.doi.org/10.1144/SPE374.8, (2012).
2. Firoozabadi A. “Recovery Mechanisms in Fractured Reservoirs and field performance”, Journal of Canadian Petroleum Technology (2000), 39 (11), 13-17.
3. Arshadi, M., M. Khishvand, A. Aghaei, M. Piri, and G. Al-Muntasheri, “Micro-Scale Investigation of Matrix-Fracture interactions in Fractured Porous Media”. (2016), *in preparation*.
4. Alajmi, A., and A. Grader, “Analysis of Fracture-Matrix Fluid Flow Interactions Using X-ray CT,” SPE 65628, Proceedings of the SPE Eastern Regional Meeting, Morgantown, West Virginia, 2000.

5. Alvarado, F., A. Grader, P. Halleck, “Visualization of two- and three-phase flow in fractures using X-ray computed tomography”. Paper SCA2006-025, Proceedings of the international symposium of the society of core analysis, Trondheim, Norway 12-16 September (2006).
6. Wildenschild, D., A. Sheppard, “X-ray imaging and analysis techniques for quantifying pore-scale structure and processes in subsurface porous medium systems”. *Advances in Water Resources* (2013), 51, 217-246, dx.doi.org/10.1016/j.advwatres.2012.07.018.
7. Alizadeh, A.H., and M., Piri, “Three-phase flow in porous media: A review of experimental studies on relative permeability”. *Reviews of Geophysics*, (2014) 52, 468-521.
8. Alizadeh, A.H., and M. Piri, “The effect of saturation history on three-phase relative permeability: An experimental study”, *Water Resources Research*, 50 (2014), 1636-1664
9. Kantzas, A., I. Chatzis, and F. Dullien, “Enhanced oil Recovery by inert gas injection”, paper SPE 17379 presented at the SPE/DOE Enhanced Oil Recovery Symposium, Soc. Of Pet. Eng., Tulsa, Ok, 17-20 Apr, (1998).
10. Zhou, D., M. Blunt, “Effect of spreading coefficient on the distribution of light non-aqueous phase liquid in the subsurface”, *Journal of Contaminant Hydrol*ogy, (1997), 25(1-2).
11. Chatzis, A., A. Kantzas, and F. Dullien, “On the investigation of gravity assisted inert gas injection using micromodels, long Berea sandstone core, and computer-assisted tomography, paper SPE 18284 presented at the SPE Annual Technical Conference and Exhibition, Soc. Of Pet. Eng., Houston TX. 2-5 Oct, (1988).
12. Vizika, O., and J. Lombard, “Wettability and spreading: Two key parameters in oil recovery with three-phase gravity drainage”, *SPE Reservoir Engineering*, (1996) 11, 1, 54-60.
13. Buckley J., Y. Xie, and N. Morrow, “Asphaltenes and crude oil wetting – the effect of oil composition” paper SPE 35366 presented at the SPE/DOE IOR symposium, Tulsa 21-24 April, (1996).
14. Alizadeh, A.H., M. Khishvand, M.A Ioannidis, and M. Piri, “Multi-scale experimental study of carbonated water injection: An effective process for mobilization and recovery of trapped oil”, *Fuel* 132 (2014), 219-235.
15. Alizadeh, A.H., and M. Piri, “Effect of saturation history on three-phase relative permeability: An Experimental Study” paper SCA2013-023, Proceedings of the International Symposium of the Society of Core Analysis, Napa Valley, California, USA, 16-19 September (2013).

Table 1: Dimensions and petrophysical properties of the core sample used in this work.

Porous medium	Length (mm)	Diameter (mm)	Porosity of the matrix (%)*	Permeability to brine (mD)*	Pore volume (ml)
Berea	40.03	9.98	20.50	1089	0.63

*Porosity and permeability of the Berea sandstone core plug (38 mm in diameter and 100 mm in length) were measured using an automated porosimeter-permeameter before inducing the fracture. The values were 21% and 842 mD, respectively.

Table 2: Properties of a fluid system [8] similar to the one used in this study.

Fluid	Viscosity (mPa.s)	Density (kg/m$^{3)}$
Brine	1.144	1138.12
Oil (Soltrol 170)	2.526	802.13
Gas (Nitrogen)	0.0187	62.84

Table 3: IFT values a fluid system [8] similar to the one used in this study.

Pair of fluids	IFT (mN/m)
Oil-brine	40.77
Nitrogen-oil	20.96
Nitrogen-brine	61.71

Table 4: Microtomography parameters used to generate pore space and fluid occupancy maps in this study.

Recipe	Projections Counts	Exposure Time (seconds)	Camera Binning	Resolution (μm)	Objective
High Res. Scan	3201	6	1	2.5	4X
Low Res. Scan	1601	1	2	5	4X
Full Scan	2401	4	2	10	0.4 X

Table 5: Physical locations imaged during various stages of the experiments.

Point of Interest (POI)	Sample	Diameter (mm)	Length (mm)	Slices Counts	Resolution (μm)
A	Pure Fracture	5	4.25	1800	2.5
B	Fracture and matrix	5	8.25	3600	2.5
C	Pure Matrix	5	4.25	1800	2.5

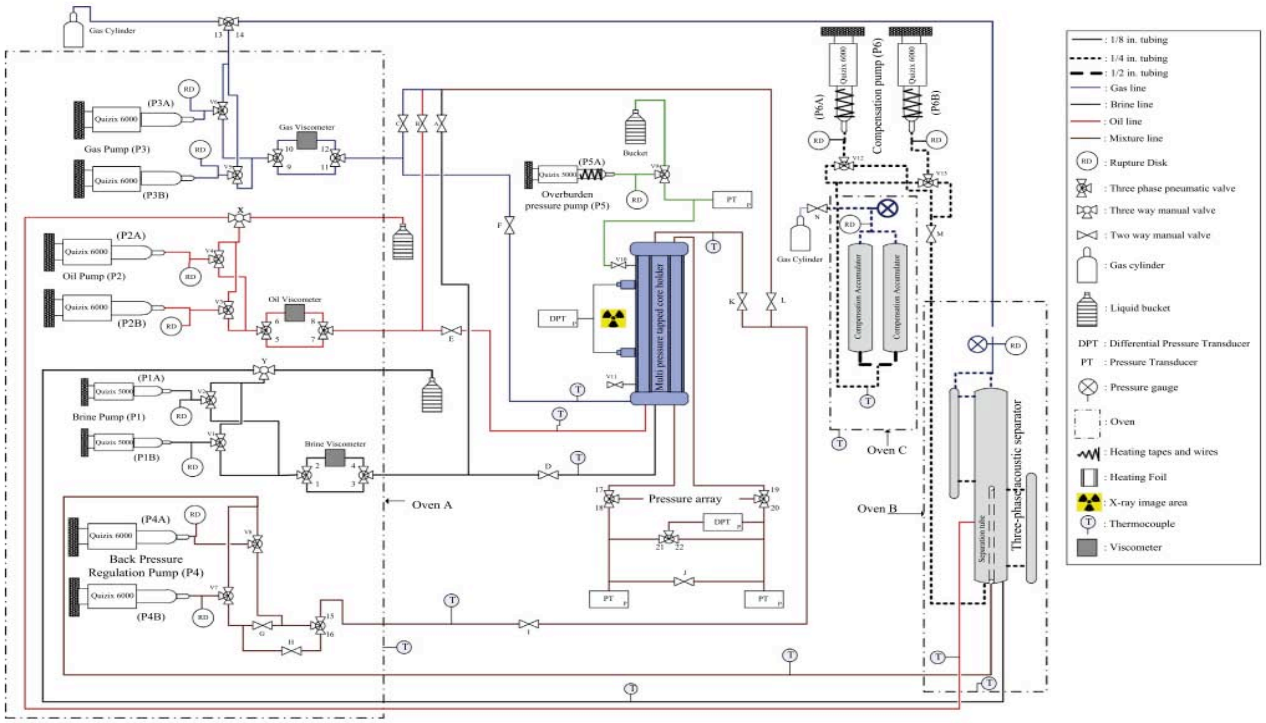

Figure 1. Schematic diagram of the experimental setup used in this study [8].

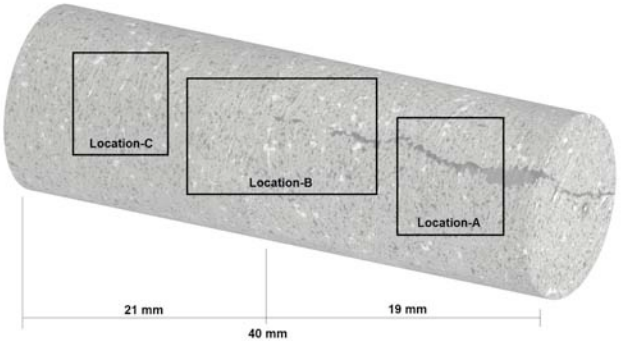

Figure 2. Three-dimensional representation of the core sample used in this study. Three locations (*i.e., A, B, and C*) were scanned during the experiments.

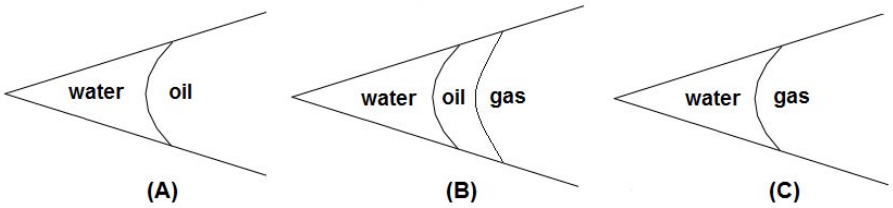

figure 3. Possible fluid configurations in a corner of a pore element with an angular cross sectional area for (A) primary drainage (oilflooding), (B) gas injection, and (C) at the end of gas injection [15].

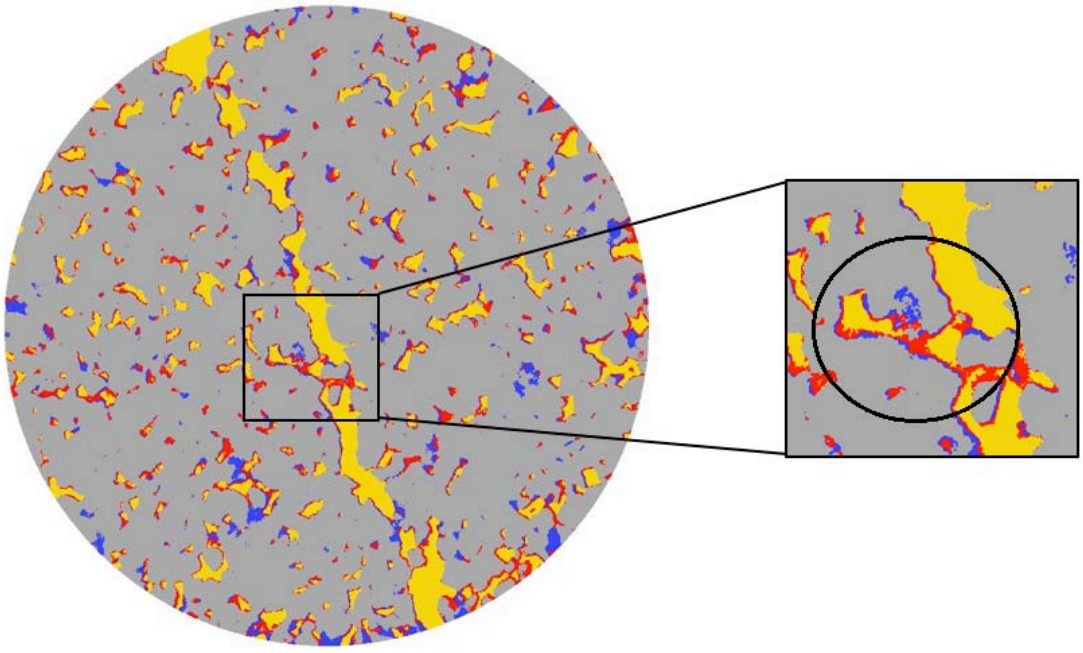

Figure 4. A segmented three-phase image showing the fluid occupancy map at a high gas flow rate (resolution: 2.5 μm). Blue, red, yellow, and gray colors represent brine, oil, gas, and grains, respectively.

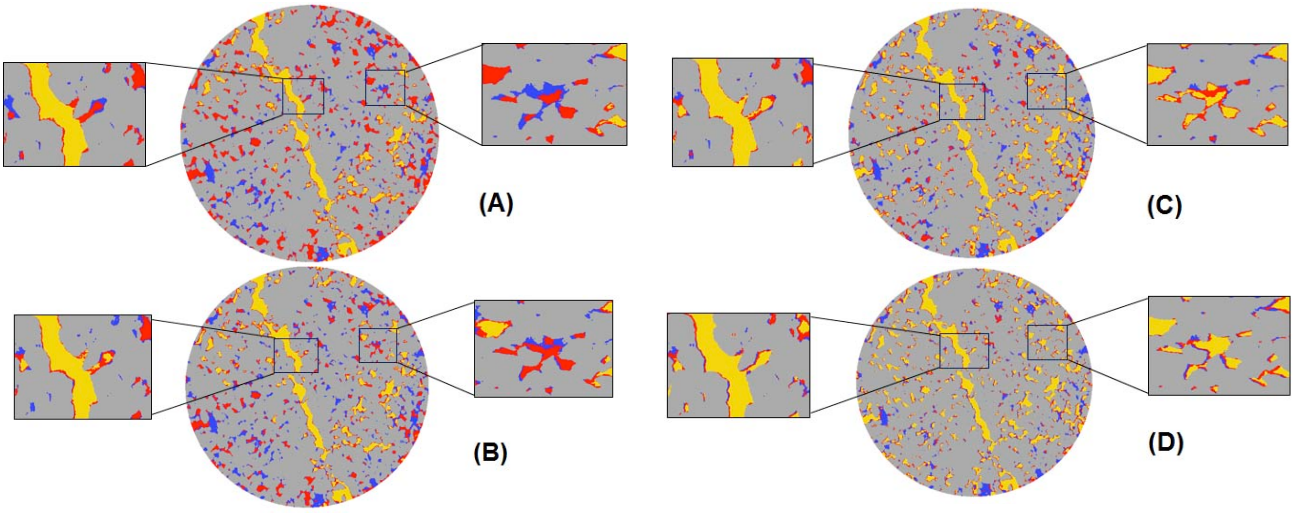

Figure 5. Segmented three-phase images showing the fluid occupancy map obtained during gas injection with a resolution of 2.5 µm. Blue, red, yellow, and gray colors represent brine, oil, gas, and grains, respectively. (A) and (B) were obtained at low gas flow rates, whereas (C) and (D) were generated at high flow rates.

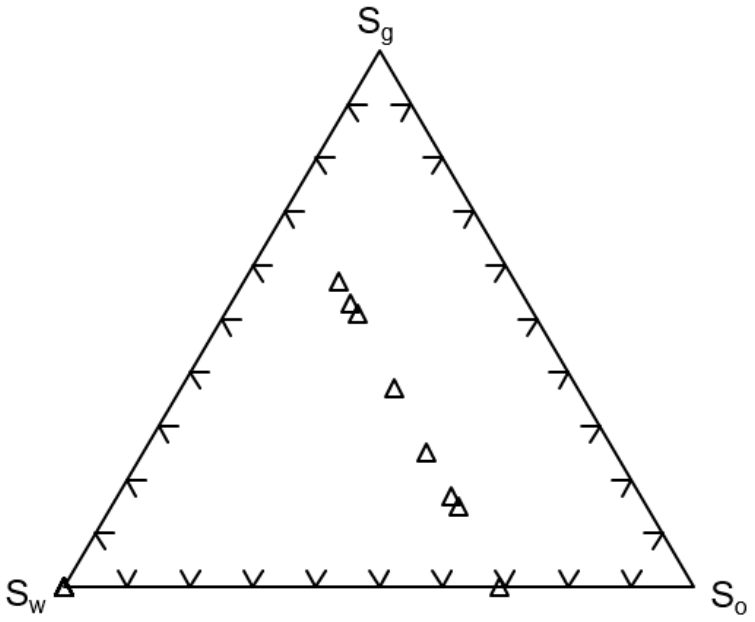

Figure 6. Saturation path taken during the experiments. The points represent fluid saturations measured at location C.